New examination of the traditional Raman Lidar technique I: temperature dependence and the calculation of atmospheric transmission

David N. Whiteman
NASA/Goddard Space Flight Center
Greenbelt, MD 20771

January 18, 2002

Abstract

The intent of this paper and its companion paper is to pull together the essential information required for the traditional Raman lidar data analysis to be performed. As a part of this, complications such as the temperature dependence of the water vapor signal is evaluated through numerical simulation. A new form of the lidar equation is presented that accounts for the temperature dependence of Raman scattering. Also the calculation of atmospheric transmission is examined carefully. Several photon correction techniques are considered as is the influence of multiple scattering on the measurement of aerosol extinction using the Raman lidar technique. OCIS # 010.3640, 010.3920, 999.9999

1 Introduction

The Raman lidar is well established today as a leading research tool in the study of numerous areas of importance in the atmospheric sciences. The Raman lidar has been used to study the passage of frontal systems [1], stratospheric aerosols due to volcanic eruptions [2], atmospheric temperature variations in cirrus clouds [3], long term variation of water vapor and aerosols at a mid-continental site [4], cloud liquid water [5], cirrus cloud optical properties [6], the influence of thin cirrus clouds on satellite retrievals of water vapor [7], hygroscopic growth of aerosols [8], cloud base height detection [9], multi-wavelength Raman lidar measurements of aerosols enabling remote characterization of aerosols [10] [11] and other topics. Recently, numerical simulation has been used to demonstrate that an airborne Raman water vapor lidar offers a dramatic increase in temporal and spatial resolution compared to existing differential absorption lidars under nighttime conditions [12]. Yet, despite the availability of several good references describing the traditional Raman lidar measurements of water vapor and aerosols [13] [14] [1] [15] [16] [17] [8] [18] [4], the essential material needed for analyzing Raman lidar data has not been compiled previously into a single reference. With several new Raman lidars being developed in Europe as a part of the European Aerosol Lidar Network (EARLINET) [19] [20], it seemed an appropriate time to create such a reference. Furthermore, and perhaps more importantly, recent work in numerical simulation of the Raman water vapor spectrum now permits the temperature sensitivity of Raman scattering from water vapor to be evaluated as it has been possible for the rotational Raman scattering from diatomic molecules [21] [3] [22] since the early days of lidar [23]. To account for this temperature sensitivity, new equations will be derived for the traditional Raman lidar quantities.

The general organization of this paper is as follows. First, as reference material, the traditional lidar equations are presented. The temperature sensitive lidar equations are developed next after which follows a detailed description of the calculation of atmospheric transmission. The equations and analysis examples for the aerosol extinction, aerosol scattering ratio, aerosol

backscattering coefficient and water vapor mixing ratio are then presented. Two appendices are included dealing with the related topics of the influence of multiple scattering on the calculation of aerosol extinction as well as correction for photon counting pulse pile-up.

The sequence of sections and their content is as follows:

Section 2 - Traditional Lidar equations

Section 3 - Temperature dependent Lidar equations, atmospheric transmission function

Section 4 - Atmospheric extinction due to molecules and aerosols, aerosol optical depth

Appendix 1 - Consideration of the influence of multiple scattering on the calculation of aerosol extinction

Appendix 2 - Detailed description of different photon counting processing techniques

2 Traditional single scattering Rayleigh-Mie and Raman lidar equations

The background-subtracted power received by a detector as a function of range in an elastic backscatter lidar system, assuming no multiple scattering, can be expressed as

$$P(\lambda_L, r) = \frac{O(r) P_0(\lambda_L) A \xi(\lambda_L) \left(N_R(r) \frac{d\sigma_R(\pi)}{d\Omega} + \beta_\pi^{aer}(\lambda_L, r) \right)}{r^2} e^{-2 \int_0^r \alpha(\lambda_L, r') dr'} \quad (1)$$

$P'(\lambda_L, r)$ is the backscattered power (after subtracting any background contribution due for example to skylight or detector noise) received at the laser wavelength , λ_L, as a function of range, r. $O(r)$ is the channel overlap function, $P_0(\lambda_L)$ is the output power of the laser at the laser wavelength, λ_L. $N_R(r)$ is the number density of "air" molecules and $d\sigma_R(\lambda_L, \pi)/d\Omega$ is the Rayleigh backscatter cross section at the laser wavelength. $\beta_\pi^{aer}(\lambda_L, r)$ is the backscatter coefficient due to aerosol (Mie) scattering at the laser wavelength and at range r and $\xi(\lambda_L)$ is the total lidar receiver optical efficiency at the laser wavelength and includes factors such as the reflectivity of the telescope, the transmission of any conditioning optics, the transmission of any filters and the quantum efficiency of the detector. A is the receiver telescope area. The exponential factor gives the two-way atmospheric transmission, where $\alpha(\lambda_L, r)$ is the total extinction coefficient due to scattering and absorption by molecules and aerosols at the laser wavelength as a function of range along the path of the laser beam. In this context, the term "aerosols" may be used to describe any non-molecular atmospheric constituent such as dust, water droplets, ice crystals, etc.

The corresponding single scattering Raman lidar equation for a Raman species X, in its traditional form, is given in equation

$$P(\lambda_X, r) = \frac{O_X(r)\ P_0(\lambda_X)\ N_X(r)\ \frac{d\sigma_X(\lambda_L,\pi)}{d\Omega} A\,\xi(\lambda_X)}{r^2} \times e^{-\int_0^r \{\alpha(\lambda_L,r') + \alpha(\lambda_X,r')\} dr'} \quad (2)$$

where now it should be noted that the transmission term includes a term at the laser wavelength, λ_L, (for the transmission along the output path) and one at the backscattered wavelength, λ_X, which has been shifted from the laser wavelength due to the inelastic Raman scattering interaction with atmospheric molecules.

2.1 Temperature dependence of the equations

Equations 1 and 2 assume that the return signal can be considered to be at a discrete wavelength. In the case of the Raman signals excited in the near UV by lasers such as the frequency tripled Nd:YAG, the desired signal actually covers an interval that can range from a few tenths of nanometers (e. g. the OH-stretch region of water vapor) to a few nanometers (rotational-vibrational spectrum from diatomic molecules such as N_2 and O_2). In the case of the elastic return, there is pure rotational Raman scattering from nitrogen, oxygen and other molecules that is centered on the laser wavelength and that covers a band of a few nanometers as well [24].

Therefore, there is Raman scattering to be considered in both the "elastic" and Raman lidar signals. The individual line strengths in a Raman spectrum are temperature dependent. In general, this temperature dependence should be considered when formulating either the elastic or Raman lidar equations since, if the filter used to make the measurements transmits any Raman signals, the intensity of the backscattered signal per molecule may be temperature sensitive.

To illustrate this, consider the case of the Raman vibrational signals. The molecules are, to a very good approximation, all in their ground state at atmospheric temperatures as determined by the Maxwell-Boltzmann distribution. A Raman scattering event is therefore overwhelmingly likely to involve a transition from the ground state to the Stokes (higher energy) part of the spectrum. Thus, at atmospheric temperatures, the integral across the entire Raman Stokes band will be temperature insensitive (the transition will appear *somewhere* in the spectrum). However, if only a portion of the band is transmitted, there will be a temperature dependence to the transmitted intensity. For the case of the pure rotational Raman scattering centered on the elastic backscatter, however, the rotational states differ little in energy from the ground state so that there is a significant probability

that some of the rotational states will be excited at atmospheric temperatures. Thus, in order for the integral of pure rotational Raman scattering to be completely temperature insensitive, it must be done across both the O and S branches of the rotational Raman scattering. Again, if only a portion of the rotational Raman O and S branches are transmitted, the return signal will be temperature sensitivity.

If the lidar system efficiency is constant over the wavelength interval containing a Raman feature, either vibrational or pure rotational, then there is no temperature sensitivity to the received signals [25]. However, if narrow filters are used in the detection of the Raman features, the total lidar system efficiency is likely to change as a function of temperature as the strengths of the individual lines in the Raman spectrum change [26]. For example, the intensities of rotational and vibrational-rotational lines from N_2 and O_2 are well predicted by the diatomic molecule line strength models. These models has been used to enable atmospheric temperature measurements using Raman lidar [22] [3] [27]. These same models can be used to calculate the temperature sensitivity of these signals for a given bandpass filter.

However, water is an asymmetric top molecule that possesses a much more complicated spectrum than does either N_2 or O_2. The numerical simulation of the spectrum from asymmetric top molecules such as water vapor has, in the past, been available to a very limited number of researchers [28] [29] [30] [31]. A recent publication [32] now makes it possible to easily simulate the Raman vibrational spectrum for water vapor over a range of temperatures. This permits the full temperature sensitivity of a Raman water vapor lidar system to be evaluated.

For example, simulated spectra of the Raman OH-stretch region of water vapor at two different temperatures are shown in figure 1.These spectra have been simulated using 0.5 cm^{-1} resolution at $200K$ and $295K$ based on the data published by Avila et. al., 1999 [32]. At the colder temperature, shown with a dashed line, the lower quantum number transitions near the band origin of 3657 cm^{-1} are more likely to be excited. Conversely, at the higher temperature the higher order quantum number transitions farther from the band origin are more likely to occur. This implies that for a narrow bandpass filter, such as the approximately 0.3 nm filter shown with a dash-dot line, the integrated intensity of the Raman feature across the transmission band will be temperature sensitive. It should be mentioned that the atmospheric feature that is typically measured by a Raman water vapor lidar is often referred to as the ν_1 band of water vapor. However, at atmospheric temperatures, this portion of the spectrum also includes contributions from ν_3, which must be considered for accurate simulations of the spectra [32]. Contributions from ν_2 or its overtones are not significant below temperatures of 400 K [33].

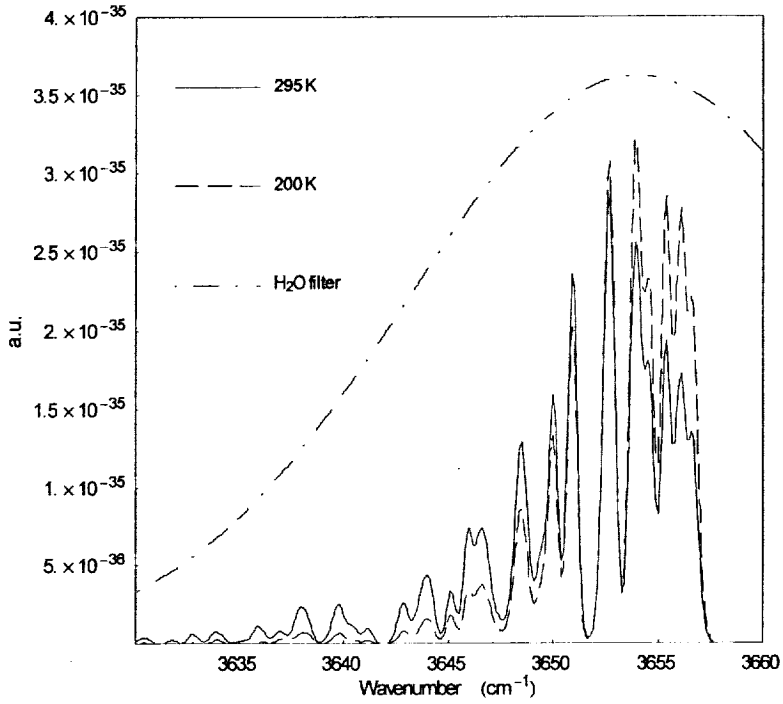

Figure 1: Raman scattering spectrum for the OH-stretch region of the spectrum simulated using a 0.5 cm^{-1} slit width and at two temperatures: 200 K and 295 K. Also shown in a representation of a 0.3 nm interference filter that could be used for the detection of the water vapor signal.

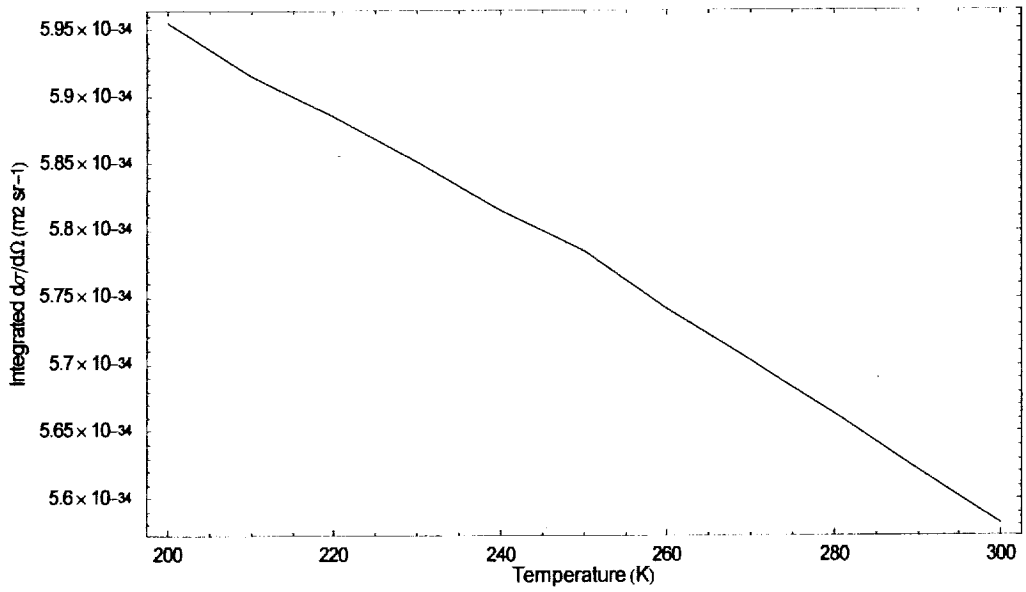

Figure 2: The integral of the Raman differential backscatter cross section and transmission of the interference filter shown in figure 1.

To illustrate the temperature sensitivity of the signal transmitted by the interference filter shown, the Raman water vapor differential backscatter cross section was determined for temperatures spanning the range of 200 - 300 K. The integral of the transmission of the interference filter shown in figure 1 and the Raman spectrum was performed at each of the temperatures. The results are plotted in figure 2. For these calculations, the area under the filter transmission curve was normalized to unity. The results shown in figure 2 indicate that there is approximately a 7% change in transmitted intensity between $200K$ and $300K$. This implies that there would be an increase in the sensitivity of a narrowband Raman lidar at high altitudes, where atmospheric temperatures are colder, compared to low altitudes.

These results suggest a reformulation of equations 1 and 2 in a manner that makes this temperature dependence more explicit. Such a reformulation has been published previously [26]. In the next section, a new formulation will be presented that permits all the temperature sensitivity of the equation to reside in a single term by which the traditional equation can be multiplied.

3 Temperature dependent lidar equations

3.1 Elastic lidar equation

The background subtracted elastic lidar equation, analogous to equation 1, but which contains the temperature dependence explicitly, is given below

$$P(\Delta\lambda_R, r) = \frac{O(r) P_0(\lambda_L) A \left(\int_{\Delta\lambda_R} \frac{N_R(r) d\sigma_R\left(\lambda', \pi, T\right)}{d\Omega} \xi\left(\lambda'\right) d\lambda' + \beta_\pi^{aer}(\lambda_L, r) \xi(\lambda_L) \right)}{r^2} e^{-2\int_0^r \alpha(\lambda_L, r') dr'} \quad (3)$$

$P(\Delta\lambda_R, r)$ is the background-subtracted, received power for the wavelength band $\Delta\lambda_R$, which contains the combined Rayleigh, Mie and rotational Raman signals, as a function of range. This is the single scattering lidar equation in a form which accounts for the possibility that the lidar system optical efficiency, $\xi\left(\lambda'\right)$, may change over the range of wavelengths $\Delta\lambda_R$. The subscript R is used to refer to the Rayleigh signal.

The Rayleigh signal consists of a narrow elastic return along with pure rotational lines, due primarily to N_2 and O_2, on both sides of the elastic line (called the "Cabannes" line by some [34] to recognize the fact that what Lord Rayleigh [35] [36] actually detected was a combination of elastic and rotational Raman scattering). These rotational Raman lines typically cover a wavelength range of a few nanometers. It is therefore possible that the lidar system transmission efficiency will change over the wavelength range $\Delta\lambda_R$. The notation $d\sigma_R\left(\lambda', \pi, T\right)/d\Omega$, which includes the explicit temperature dependence, is thus used for the differential backscatter cross section for the combined effects of elastic and pure rotational Raman scattering. This formulation allows the influence of the changing intensity of the rotational Raman lines as a function of temperature to be quantified. These changes can introduce a temperature sensitivity to the Rayleigh signal. Calculations of the rotational Raman line intensities of these diatomic molecules as a function of temperature [22] [3] [21] coupled with knowledge of the bandpass filter transmission characteristics is needed to evaluate the temperature dependence of equation 3. (Pure rotational scattering from other molecules such as water vapor [37] and carbon dioxide also exist but at such a small level as to be insignificant for the present purposes.)

Aerosols in the atmosphere are much heavier than molecules. The Doppler broadening of the return signal due to aerosols will therefore be much less than that for molecules. Because of this, the elastic scattering due to aerosols (Mie scattering) has a narrower spectral width than the elastic scattering from molecules. Thus, the single wavelength notations used in the traditional lidar equation of $\beta_\pi^{aer}(\lambda_L, r)$, for the backscatter coefficient due to aerosol scattering, and $\xi(\lambda_L)$, for the total receiver system efficiency at the laser wavelength, are still appropriate in the temperature dependent form of the equation. At the spectral resolution of a typical Raman Lidar system, it is not necessary to consider an interval over $\Delta\lambda$ for the elastic scattering from

either aerosols or molecules.

3.2 Raman lidar equation

The temperature dependent equation for the signal from a vibrationally excited Raman species X is

$$P(\Delta\lambda_X, r) = \frac{O_X(r)\ P_0(\lambda_L)\ N_X(r)\ A\ \int_{\Delta\lambda_X} \frac{d\sigma_X\left(\lambda', \pi, T\right)}{d\Omega}\ \xi\left(\lambda'\right)\ d\lambda'}{r^2} \times e^{-\int_0^r \{\alpha(\lambda_L, r') + \alpha(\lambda_X, r')\} dr'} \tag{4}$$

where now $\Delta\lambda_X$ refers to the wavelength interval over which the Raman vibrational signal is detected. Notice here the lack of the aerosol backscatter term $\beta_\pi^{aer}(\lambda_L, r)\,\xi(\lambda_L)$ since only inelastically scattered radiation due to molecular interactions is present in this signal. A temperature dependent function will now be introduced that will permit equations 3 and 4 to be expressed in a manner that will simplify the upcoming derivations.

3.3 The function $F_X(T)$

Consider the case of the Raman scattered signal from water vapor expressed by equation 4 by replacing X by H. The integral over $\Delta\lambda_H$ may be expressed as

$$\int_{\Delta\lambda_H} \frac{d\sigma_H\left(\lambda', \pi, T\right)}{d\Omega}\ \xi\left(\lambda'\right)\ d\lambda' = F_H(T) \frac{d\sigma_H(\pi)}{d\Omega}\ \xi_{filter}(\lambda_H)\ \xi'(\lambda_H) \tag{5}$$

So that $F_H(T)$ becomes:

$$F_H(T) = \frac{\int_{\Delta\lambda_H} \frac{d\sigma_H\left(\lambda', \pi, T\right)}{d\Omega}\ \xi\left(\lambda'\right)\ d\lambda'}{\frac{d\sigma_H(\pi)}{d\Omega}\ \xi_{filter}(\lambda_H)\ \xi'(\lambda_H)} \tag{6}$$

A new function $F_H(T)$ has been introduced which carries all the temperature dependence of the lidar equation. It contains the effects of any changes in the system transmission efficiency, $\xi(\lambda)$, for wavelengths other than λ_H within the band $\Delta\lambda_H$, which will be assumed to cover the entire Raman spectrum. The notation $d\sigma_H(\pi)/d\Omega$ is used to indicate the total Raman backscatter cross section for water vapor at the stimulating wavelength. For the XeF laser (351 nm) based measurements used in this paper that value is approximately 6.2 $\times 10^{-34}\ m^2 sr^{-1}$ [24] (which, at atmospheric temperatures, is essentially constant with temperature). The interference filter transmission efficiency, ξ_{filter}, at the center wavelength, λ_H, of the Raman feature has been

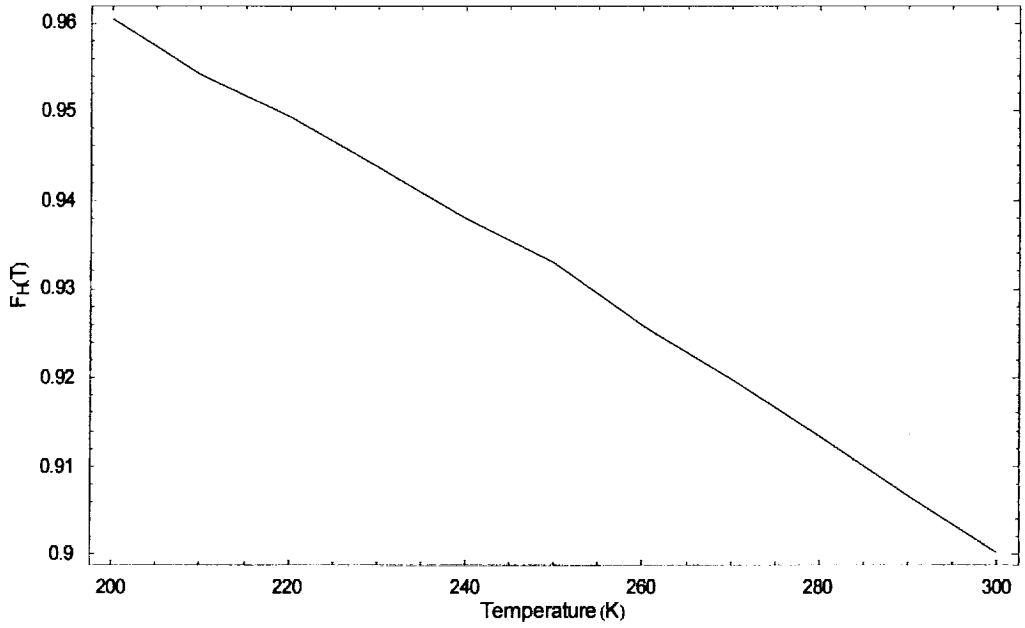

Figure 3: The function $F_H(T)$ from equation 5 for the case of the interference filter shown in figure 2. For illustration purposes, this plot assumes that all the wavelength variation of the lidar receiver optical efficiency is due to the interference filter.

separated from the transmission of the remaining optical components, $\xi'(\lambda_H)$. This was done as a practical matter since filter transmissions are often evaluated separately from the optical transmission of the remaining lidar system. Also, in a well designed lidar system, the filter transmission will be the source of most of the variation in system transmission over $\Delta\lambda_H$.

Data such as presented in figure 1 may now be used to illustrate the calculation of $F_H(T)$ for the case of a water vapor measurement using the 0.3 nm filter also shown in the figure. Similar calculations can be done for the diatomic molecules using the previously cited references. Consider the simplifying case of $\xi'(\lambda_H)$ equal to a constant (taken to be unity for simplicity) on the right hand side of 5 so that all variation in system transmission over the interval $\Delta\lambda_H$ is due to the optical filter. This is a good approximation for a properly designed lidar system. Thus the function $F_H(T)$ given in equation 6 may be determined by dividing the values shown in figure 2, which corresponds to the numerator of 6, by the product of the total backscatter cross section $d\sigma_H(\pi)/d\Omega$ and the peak filter transmission efficiency $\xi_{filter}(\lambda_H)$ (taken also to be unity for simplicity). The results are in figure 3 indicating that the interference filter shown in figure 1, assuming a peak filter transmission of 1.0, will transmit between 90% - 96% of the full Raman water vapor band over the range of temperatures considered.

3.4 New formulation of the single scattering Lidar equations containing temperature sensitivity

Using this simplified formulation of the temperature sensitivity, the single-scattering elastic and Raman lidar equations can be expressed as follows

$$P(\Delta\lambda_R, r) = \frac{O(r)\ F_R(T)\ P_0(\lambda_L)\ A\,\xi(\lambda_L)\left(\beta_\pi^{mol}(\lambda_L, r) + \beta_\pi^{aer}(\lambda_L, r)\right)}{r^2} \times e^{-2\int_0^r \alpha(\lambda_L, r')dr'} \tag{7}$$

$$P(\Delta\lambda_X, r) = \frac{O_X(r)\ F_X(T)\ P_0(\lambda_L)\ A\ N_X(r)\ \frac{d\sigma_X(\pi)}{d\Omega}\ \xi(\lambda_X)}{r^2} \times e^{-\int_0^r \{\alpha(\lambda_L, r') + \alpha(\lambda_X, r')\}dr'} \tag{8}$$

where $\beta_\pi^{mol}(\lambda_L, r) = N_R(r)\ d\sigma_R(\pi)/d\Omega$, $d\sigma_R(\pi)/d\Omega$ is the full Rayleigh cross section including the effects of rotational Raman scattering, the filter transmissions are now contained within the efficiency terms $\xi_X(\lambda)$ and in the case of the elastic equation the assumption has been made that the interference filter is centered on the laser wavelength. These forms of the lidar equations will be used in the derivations to come after considering the calculation of the transmission terms in the lidar equations.

3.5 The atmospheric transmission function

The atmospheric transmission function for the Raman lidar equation, $\exp[-\int_0^r \{\alpha(\lambda_L, r') + \alpha(\lambda_X, r')\}dr']$, accounts for the fact that photons are transmitted into the atmosphere by the laser at wavelength, λ_L, and return at the Raman shifted wavelength, λ_X, for Raman species X. (The Rayleigh case is handled simply by setting $X = L$.) Since the atmospheric extinction is different at these wavelengths, the transmission factor must account for this. The extinction that occurs at a certain wavelength is, in general, due to both scattering and absorption from both aerosols and molecules in the atmosphere. The total extinction coefficient is therefore given by aerosol and molecular contributions

$$\alpha(\lambda, r) = \alpha_{aer}(r) + \sum_{i=1}^{M} N_i(r)\left[\sigma_i(\lambda) + \eta_i(\lambda)\right] \tag{9}$$

In this equation, $\alpha(\lambda, r)$ is the total extinction at wavelength λ and range r, $\alpha_{aer}(r)$ is the extinction due to aerosol scattering

and absorption, $N_i(r)$ is the molecular number density of the i^{th} scatterer or absorber, $\sigma_i(\lambda)$ is the total scattering cross section for the i^{th} molecule and $\eta_i(\lambda)$ is the absorption cross section for the i^{th} molecule. M is the total number of different molecules being considered. For a typical Raman lidar using a UV laser such as the XeF excimer (351 nm) or the frequency-tripled Nd:YAG (355 nm), the wavelength range of the return signals is approximately 350 - 410 nm, a region of the spectrum where molecular absorption is negligible [38]. For the purposes of the data analysis to be presented later, the molecular component of the atmospheric extinction coefficient $\alpha(\lambda, r)$ is therefore due only to scattering by the various molecules in the atmosphere. Thus, the following equation for the extinction coefficient applies

$$\alpha(\lambda, r) = \alpha_{aer}(r) + \sum_{i=1}^{M} N_i(r)\,\sigma_i(\lambda) \tag{10}$$

Typical Rayleigh scattering formulas provide a composite cross section for the collection of molecules that make up normal air. Using this fact to re-express the equation yields

$$\alpha(\lambda, r) = \alpha_{aer}(r) + N_{air}(r)\,\sigma_{air}(\lambda) \tag{11}$$

4 Atmospheric extinction due to molecules and aerosols

In order to evaluate the atmospheric transmission function appropriate for the typical UV or visible Raman lidar, we need to evaluate separately the contributions due to molecular and aerosol extinction.

4.1 Molecular extinction

In the absence of absorption, extinction of the laser beam is entirely due to scattering. An excellent treatment of Rayleigh scattering in the atmosphere is given by Bucholtz [39]. Those results have been used here to calculate Rayleigh extinction. Equation 12 gives the cross section per molecule for Rayleigh scattering [39].

$$\sigma(\lambda) = \frac{24\pi^3 \left(n_s^2 - 1\right)^2}{\lambda^4 N_s^2 \left(n_s^2 + 2\right)^2} \left(\frac{6 + 3\rho_n}{6 - 7\rho_n}\right) \tag{12}$$

where $\sigma(\lambda)$ is the cross section per molecule (in units of cm^2) at the wavelength $\lambda(cm)$, n_s is the refractive index for dry air at standard temperature and pressure (STP), N_s is the molecular number density for air at STP (2.547 x 10^{19} cm^{-3}) and ρ_n is the

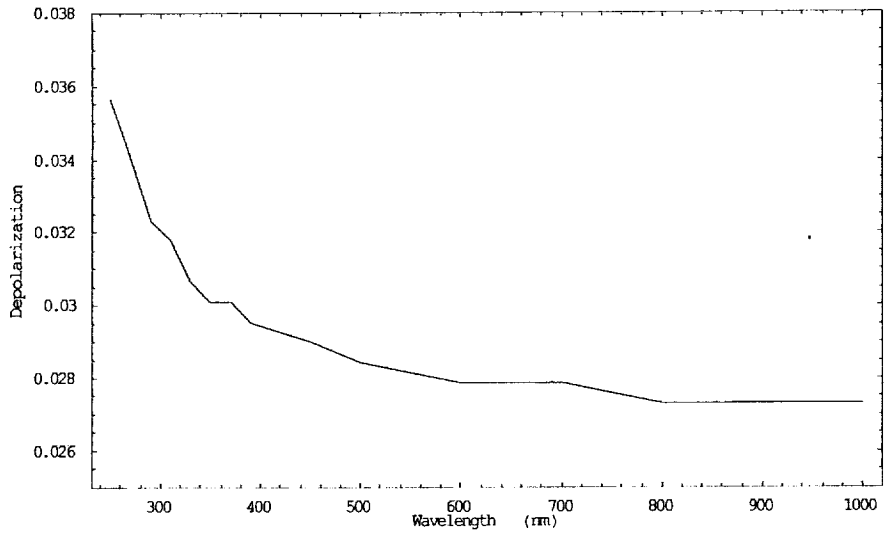

Figure 4: Variation of the Rayleigh depolarization ratio as a function of wavelength from the near UV to the near IR from reference [39]. An accurate quantification of Rayleigh scattering should account for this varation in depolarization.

depolarization ratio defined as

$$\rho_n \equiv \frac{I_s^{\perp}}{I_s^{\parallel}} \tag{13}$$

where $I_s^{\parallel}$ and $I_s^{\perp}$ are the scattered intensities in directions parallel and perpendicular to the polarization direction of the incident linearly polarized bream. The Rayleigh depolarization ratio changes as a function of wavelength as shown in figure 4. These results take full account of the depolarization of the Rayleigh signal due to rotational Raman scattering [39].

Other formulations of the Rayleigh cross section [24] assumed a constant depolarization ratio. However, it actually changes by 30% between 250 nm and 1000 nm when the influence of rotational Raman scattering is included. As will be shown later, these formulations can differ significantly.

The refractive index of air at standard temperature and pressure (STP) may be calculated from the following empirical formula [40] for wavelengths greater than 230 nm [39].

$$n_s = 10^{-8}\left(\frac{5791817}{238.0185 - (1/\lambda)^2} + \frac{167909}{57.362 - (1/\lambda)^2}\right) + 1 \tag{14}$$

It is interesting to compare the values of total Rayleigh cross section given by equations 12 and 14 and a simpler formulation [24] given by

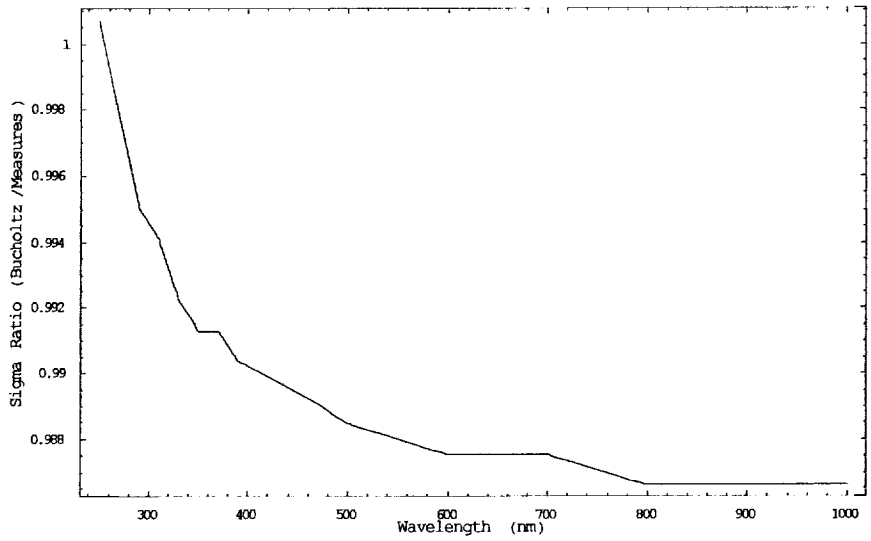

Figure 5: Ratio of two formulations of total Rayleigh scattering cross section. The simpler formulation from Measures [24] assumes that $\left(n_s^2+2\right) = 3$ and assumes that the depolarization of air is constant with wavelength. The formulation from Bucholtz [39] does not make these assumptions.

$$\sigma_{simpler}(\lambda) = \frac{8\pi^3\left(n_s^2-1\right)^2}{3\lambda^4 N_s^2}\left(\frac{6+3\rho_n}{6-7\rho_n}\right) \tag{15}$$

where the depolarization is considered constant and where $\left(n_s^2+2\right)$ is taken to be equal to 3. Figure 5 compares these two formulations for the case of $\rho_n = 0.035$ [24]. As the figure shows the dispersion of polarization changes the Rayleigh cross section by approximately 1% across the wavelength range of 250 - 800 nm. Furthermore, the more complete formulation from Bucholtz yields values approximately 1% lower than the simpler formulation in the critical wavelength region above 350 nm.

The total Rayleigh volume-scattering coefficient as a function of wavelength at STP is now given by [39]

$$\beta_s = N_s\sigma(\lambda)\ \left(cm^{-1}\right) \tag{16}$$

For any pressure, temperature or number density, the Rayleigh volume scattering coefficient may be determined from [39]

$$\beta = N\sigma(\lambda) = \beta_s\frac{N}{N_s} = \beta_s\frac{P}{P_s}\frac{T_s}{T} \tag{17}$$

where β_s, P_s and T_s are calculated at STP. In the absence of absorption, molecular extinction is determined completely by Rayleigh scattering and thus the molecular component of the atmospheric extinction coefficient $\alpha(\lambda, r)$, from equation 11, is given by equation 17. The intensity of Rayleigh backscattering is independent of laser polarization so that polarization need not

be considered here.

4.2 Aerosol extinction

To compute aerosol extinction analytically generally requires knowledge of the exact nature of the aerosols that are responsible for the extinction. Given the size distribution of the aerosols as a function of range and both real and imaginary indices of refraction, a calculation using Mie theory can be performed which will estimate the extinction as a function of range. This can be done very accurately for non-precipitating cloud water droplets, which are spherical, provided that multiple scattering is not significant. But for other aerosols, which can have irregular shapes that are usually not known, calculations of aerosol scattering properties using Mie theory are approximations at best.

However, with the Raman lidar, another approach to the calculation of aerosol extinction is possible. The Raman nitrogen (or oxygen) signal may be used to calculate the round-trip atmospheric extinction (which occurs at the laser wavelength for the outgoing path and at the Raman shifted wavelength for the return path) directly.

4.2.1 Development of the extinction equations including the effects of temperature sensitivity

Aerosol extinction can be quantified in a direct manner by using either the Raman nitrogen or oxygen signals [41]. At the ultra-violet and visible wavelengths of the lasers typically used in the Raman lidar systems SRL, atmospheric absorption is negligible so aerosol extinction is determined by the total amount of light scattered into all directions. This is the integral of the aerosol scattering phase function and quantifies an important radiative property of the aerosols. The equation for calculating the aerosol extinction from Raman lidar data can be derived along similar lines as in Ansmann et. al. [41] except that the current equations include the influence of the temperature sensitivity of Raman scattering. Assuming the use of the Raman nitrogen signal for the calculation of aerosol extinction, the result is

$$\begin{aligned} & \alpha_{aer}(\lambda_L, r) + \alpha_{aer}(\lambda_N, r) \\ = \; & \frac{d}{dr}\left[\ln\left(\frac{O_N(r)\; F_N(T)\; N_N(r)}{r^2\; P(\lambda_N, r)}\right)\right] - \alpha_{mol}(\lambda_L, r) - \alpha_{mol}(\lambda_N, r) \end{aligned} \tag{18}$$

where $\alpha_{aer}(\lambda_L, r)$ is the extinction due to aerosols on the outgoing path at the laser wavelength, $\alpha_{aer}(\lambda_N, r)$ is the aerosol extinction on the return path at the Raman shifted wavelength, $\alpha_{mol}(\lambda_L, r)$ is the molecular extinction at the laser wavelength,

and $\alpha_{mol}(\lambda_N, r)$ is the molecular extinction at the Raman shifted wavelength.

Equation 18 is the fundamental Raman lidar aerosol extinction equation. It is identical to the results of Ansmann et. al. [41] except or the inclusion of the temperature dependent factor $F_N(T)$. The atmospheric number density is required to evaluate this equation both for the calculation of the molecular extinction terms (through the use of equation 17) as well as to evaluate the number density $N_N(r)$. In the lowest ~100 km of the atmosphere the total atmospheric density is proportional to $N_N(r)$ and thus gives identical results in the equation. The sensitivity of Raman measurements of aerosol extinction to changes in atmospheric temperature and density variations has been studied by Ansmann et. al. [41]. Their conclusion was that the use of a standard atmospheric model for calculating molecular extinction can introduce significant errors in aerosol extinction when the aerosol loading is very low. Therefore the more accurate molecular number density profile available from a radiosonde is recommended under such conditions.

Equation 18 indicates that the fundamental quantity that can be evaluated using a Raman lidar is the two-way extinction that occurs along the round-trip path from the laser to a scattering element and back to the telescope. In order to translate this into one-way extinction at a single wavelength, knowledge of the wavelength scaling of aerosol extinction is needed. The scaling of aerosol extinction may be handled as follows [42]

$$\frac{\alpha_{aer}(\lambda_L, r)}{\alpha_{aer}(\lambda_N, r)} = \left(\frac{\lambda_N}{\lambda_L}\right)^{k(r)} \tag{19}$$

where k may vary between approximately 0 and 2 depending on the nature of the aerosols [8] and is a function of range. Using equation 19, the expression for aerosol extinction at the laser wavelength becomes

$$\alpha_{aer}(\lambda_L, r) = \frac{\frac{d}{dr}\left[\ln\left(\frac{O_N(r)\, F_N(T)\, N_N(r)}{r^2\, P(\lambda_N, r)}\right)\right] - \alpha_{mol}(\lambda_L, r) - \alpha_{mol}(\lambda_N, r)}{1 + \left(\frac{\lambda_L}{\lambda_N}\right)^{k(r)}} \tag{20}$$

An alternate form of this equation, which is preferred since it allows Gaussian distributed quantities to be regressed when determining the numerical derivative [43] can be derived by noting that

$$\begin{aligned} &\frac{d}{dr}\left(\ln\left[\frac{O_N(r)\; F_N(T)\; N_N(r)}{r^2 P(\lambda_N, r)}\right]\right) \\ &= \frac{1}{O_N(r)}\frac{d}{dr}O_N(r) + \frac{1}{F_N(T)}\frac{d}{dr}F_N(T[r]) + \frac{1}{N_N(z)}\frac{d}{dz}N_N(z) - \frac{1}{r^2 P(\lambda_N, r)}\frac{d}{dr}[r^2 P(\lambda_N, r)] \end{aligned} \tag{21}$$

where it has been explicitly noted that temperature is a function of range. Using this expression in equation 20 yields

$$\alpha_{aer}(\lambda_L, r) = \frac{\frac{1}{O_N(r)}\frac{d}{dr}O_N(r) + \frac{1}{F_N(T)}\frac{d}{dr}F_N(T[r]) + \frac{1}{N_N(r)}\frac{d}{dr}N_N(r) - \frac{1}{r^2 P(\lambda_N, r)}\frac{d}{dr}[r^2 P(\lambda_N, r)] - \alpha_{mol}(\lambda_L, r) - \alpha_{mol}(\lambda_N, r)}{1 + \left(\frac{\lambda_L}{\lambda_N}\right)^{k(r)}} \tag{22}$$

As described in [43], the technique of least squares fitting assumes that the data to be regressed are normally distributed. The use of equation 22 permits all quantities to be regressed to retain their original statistical distributions, assumed to be Gaussian or near-Gaussian. This equation, therefore, is preferred to equation 20 for evaluating aerosol extinction since the ratio of two Gaussian distributed quantities does not have a Gaussian distribution.

In principle, this equation can be used over the entire range of the lidar profile to evaluate the aerosol extinction. However, in practice it is quite difficult to quantify the lidar channel overlap function sufficiently well to apply equation 22 in the overlap region. This is due to the fact that the derivative of the natural logarithm of the overlap must be evaluated. In the overlap region, the signal may be changing very rapidly so that small errors in quantifying the overlap function can introduce large errors in the derived aerosol extinction. For this reason calculations of aerosol extinction are typically performed on the portion of the lidar profile that is fully overlapped, i.e. where $O_N(r) = 1$. It should be noted as well that since the extinction will typically be evaluated over relatively short ranges (i.e. dr will in general be on the order of 100 meters), $F_N(T)$ may be considered essentially constant for the normal atmospheric measurements to be considered here. This is the case since $F_N(T)$ is generally a mild function of temperature, which typically changes little over a range of 100 m. For measurements of extinction in a smoke stack or in the vicinity of flames this would not be the case, however. In this equation the atmospheric density as a function of range will work just as well as $N_N(r)$ since they are related by a constant factor in the lower atmosphere.

Before evaluating equation 22 for the case of tropospheric aerosols, the possible influence of multiple scattering on these measurements must be addressed. Tropospheric aerosols range in size from less than 0.1 μm in radius up to 10 μm and larger in some cases [52]. The multiple scattering due to aerosols in this size range is studied in appendix 1 with the results that, for the aerosol extinction measurements presented here, multiple scattering is negligible.

4.2.2 Evaluation of the extinction equation

The evaluation of equation 22 appears to be rather straightforward once all the required quantities are known. However, the derivative term actually presents subtle and quite important difficulties relating to the proper statistical approach to evaluating

a derivative, which is defined only for continuous functions, for a set of discrete points. The statistical rules pertaining to determining the best mathematical model for fitting a set of data can be applied with good result. This procedure is described in [43].

4.2.3 Extinction due to tropospheric aerosols

An example of aerosol extinction computed from data acquired by the NASA/GSFC Scanning Raman Lidar during the third Convection and Moisture Experiment (CAMEX-3) [7] on the night of August 26, 1998 at Andros Island, Bahamas is shown in figure 6. The results shown were obtained from the raw Raman lidar measurement of molecular nitrogen by first correcting for the finite photon counting bandwidth, subtracting the background and then applying equation 22. Various photon counting correction techniques are reviewed in appendix 2. The wide spectral bandwidths used for these XeF excimer laser based measurements imply that the temperature sensitivity of Raman signal is negligible for these CAMEX-3 measurements [25].

The aerosol extinction profiles shown use a 20-minute summation of data. The molecular extinction coefficients were derived using equation 17 and atmospheric density measured by a radiosonde launched that night. In the figure, the influence of the aerosol scaling parameter (known as the Angstrom coefficient) is also tested.

Figure 6 shows a typical aerosol profile from Andros Island during the CAMEX-3 campaign. The values of extinction below ~0.25 km are influenced by the lidar overlap function. Changing the Angstrom coefficient (considered constant with range) from k=0 to k=2 increases the aerosol extinction values by approximately 8%. It has a comparable effect on the aerosol optical depth between 0.25 and 3 km which may be calculated by simply integrating the extinction curve over this altitude range. Using k=1, the aerosol optical thickness (at 351 nm) between 0.25 and 3 km was approximately 0.13 for this example.

The uncertainty in the Angstrom coefficient can be reduced by using coincident sun photometer data if available. The uncertainty in the Angstrom coefficient determined using a sun photometer is a function of the wavelength interval used to determine the coefficient, the aerosol optical depth and the quality of the calibration of the instrument in use. In general, for instruments in the NASA/GSFC Aeronet (http://aeronet.gsfc.nasa.gov:8080/), uncertainty in Angstrom coefficient will be less than ± 0.2 for the 340-380 nm wavelength interval if the aerosol optical thickness is greater than 0.4 [44] [45]. Due to the existence of an Aeronet reference standard at NASA/GSFC, a ± 0.2 uncertainty in Angstrom coefficient is obtained for aerosol optical depths greater than 0.2 [46]. It is estimated that uncertainty in the value of k contributes an error of 5% or less to these aerosol extinction measurements.

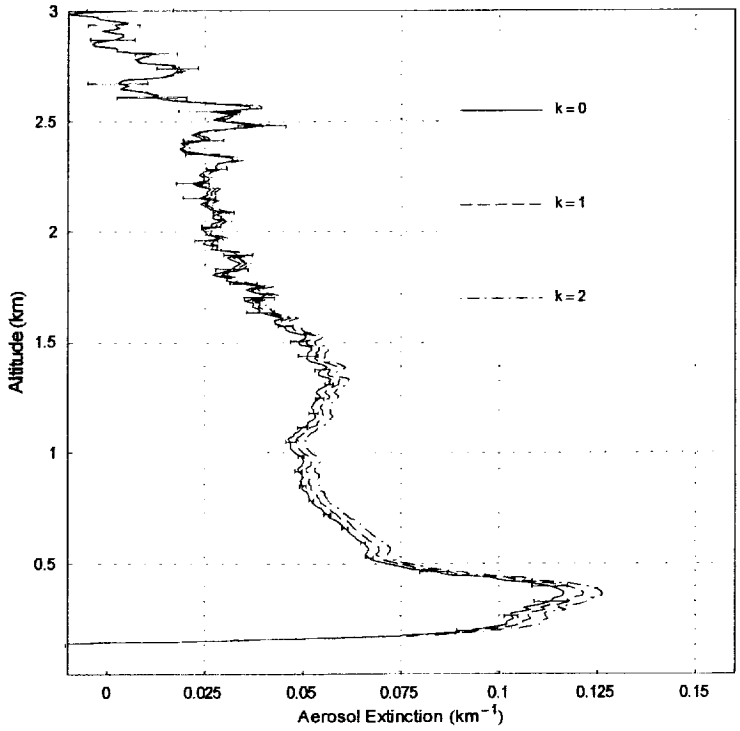

Figure 6: Aerosol extinction (at 351 nm) calculated from a 20 minute average of data from the night of August 26, 1998 at Andros Island, Bahamas. The data were acquired at an angle of 10 degrees above the horizon to improve the signal to noise. The resolution of the derived extinction values is approximately 150 m. The sensitivity of the aerosol scaling parameter is tested here.

The aerosol optical depth of ~0.13 in the current example implies that approximately 12% of the light was scattered from the beam due to aerosols ($e^{-0.13} \cong 0.88$). These measured values of aerosol extinction in the UV can be used to estimate the horizontal visibility experienced by ground-based observers. The "visual range" may be estimated from the empirical formula [24]

$$\alpha(\lambda) \approx \frac{3.91}{R_v} \left\{ \frac{550}{\lambda(nm)} \right\}^k \ (km^{-1}) \tag{23}$$

where α is the total atmospheric extinction coefficient and R_v is the visual range. At visible wavelengths and under most aerosol loading conditions, aerosol extinction is the dominant source of atmospheric attenuation [24]. For example, near the surface in figure 6, aerosol extinction at 351 nm was approximately 0.1 km^{-1}. Scaling this value to 550 nm using equation 19 and $k = 1$ yields an aerosol extinction at 550 nm of approximately 0.06 km^{-1}. By contrast, molecular extinction under standard temperature and pressure conditions, using equation 16 is approximately 0.01 km^{-1}. Using these values in equation 23, yields a value of visual range in excess of 50 km. The aerosol loading present on August 26 was typical for Andros Island during CAMEX-3 implying that aerosol optical depths were low and visibilities were generally very good.

This example demonstrates that the aerosol optical depth is an important parameter than influences visibility and thus radiative transfer. As demonstrated above, the optical depth can be determined by integrating the aerosol extinction profile. When calculating the optical depth in this manner, however, errors at all levels in the extinction profile must be added together to determine the error budget for the optical depth calculation. This can result in a larger uncertainty in the determination of the optical depth than the more straightforward calculation which will now be presented.

4.2.4 Aerosol optical depth

Integrating both sides of equation 18 over the range $\{r_1, r_2\}$ yields the two way aerosol optical depth between r_1 and r_2 :

$$\begin{aligned} & \int_{r_1}^{r_2} \left[\alpha(\lambda_L, r) + \alpha(\lambda_N, r)\right] \, dr \\ = & \left[\ln\left(\frac{O_N(r)\ F_N(T)\ N_N(r)}{r^2\ P(\lambda_N, r)}\right)\right]_{r_1}^{r_2} - \int_{r_1}^{r_2} \left[\alpha_{mol}(\lambda_L, r) + \alpha_{mol}(\lambda_N, r)\right] \, dr \end{aligned} \tag{24}$$

The use of the right hand side of equation 24 to calculate aerosol optical depth eliminates the need to perform a derivative of the lidar signal. This simplifies calculations when all that is needed is the mean value of extinction through a layer such as is

required to calculate optical depth.

The error in optical depth is calculated using the following formulas [47]:

$$x = au \pm bv : \sigma_x^2 = a^2\sigma_u^2 + b^2\sigma_v^2 \tag{25}$$

$$x = \pm auv : \frac{\sigma_x^2}{x^2} = \frac{\sigma_u^2}{u^2} + \frac{\sigma_v^2}{v^2} \tag{26}$$

$$x = \pm\frac{au}{v} : \frac{\sigma_x^2}{x^2} = \frac{\sigma_u^2}{u^2} + \frac{\sigma_v^2}{v^2} \tag{27}$$

$$x = a\ln(\pm bu) : \sigma_x^2 = a^2\frac{\sigma_u^2}{u^2} \tag{28}$$

In these formulas, u and v are functions of the independent variable while a and b are constants and the assumption has been made that the covariance between u and v is zero. Applying these error propagation equations to equation 24 yields

$$\sigma^2_{AerosolOD} \simeq \frac{\sigma^2_{O_N(r_2)}}{O_N^2(r_2)} + \frac{\sigma^2_{O_N(r_1)}}{O_N^2(r_1)} + \frac{\sigma^2_{F_N(T(r_2))}}{F_N^2(T(r_2))} + \frac{\sigma^2_{F_N(T(r_1))}}{F_N^2(T(r_1))} + \frac{\sigma^2_{N_N(r_2)}}{N_N^2(r_2)} + \frac{\sigma^2_{N_N(r_1)}}{N_N^2(r_1)} + \frac{\sigma^2_{P(\lambda_N,r_2)}}{P^2(\lambda_N,r_2)} + \frac{\sigma^2_{P(\lambda_N,r_1)}}{P^2(\lambda_N,r_1)} + 2\sigma^2_{MolecularOD} \tag{29}$$

where, to be clear, it should be noted that in this equation, $\sigma^2_{AerosolOD}$, refers to the variance of the two-way aerosol optical depth and $\sigma^2_{MolecularOD}$ refers to the variance of the one-way molecular optical depth. The variance of the $\sigma^2_{F_N(T[r])}$ terms will likely be correlated between r_1 and r_2 since the same spectral transmission data for the lidar (along with their attendant errors) will be used at both r_1 and r_2. This implies that a sensitivity analysis is perhaps the best way to quantify errors in optical depth due to uncertainties in $F_N(T)$. But since $F_N(T)$ will vary little over typical ranges of optical depth calculations in the normal atmosphere, it should contribute at most a small amount to the total error. Thus, it can be considered negligible over ranges where the temperature does not change appreciably. Furthermore, if the calculation is done outside the region where the overlap function is an influence the error equation reduces to

$$\sigma^2_{AerosolOD} \simeq \frac{\sigma^2_{N_N(r_2)}}{N_N^2(r_2)} + \frac{\sigma^2_{N_N(r_1)}}{N_N^2(r_1)} + \frac{\sigma^2_{P(\lambda_N,r_2)}}{P^2(\lambda_N,r_2)} + \frac{\sigma^2_{P(\lambda_N,r_1)}}{P^2(\lambda_N,r_1)} + 2\sigma^2_{MolecularOD} \tag{30}$$

Radiosonde density errors are generally less than 2% [48]. This can be used to simplify this equation since the error in the radiosonde data will determine the error budget for three of the terms above. Also, for a lidar system such as the SRL that uses photon counting data acquisition, Poisson statistics applies so that the variance in a measurement equals the accumulated number

of counts of the measurement itself. Putting these together yields

$$\sigma^2_{AerosolOD} \lesssim \frac{1}{P(\lambda_N, r_2)} + \frac{1}{P(\lambda_N, r_1)} + 4\ RadErr^2 \tag{31}$$

where $RadErr$ indicates the fractional error in the radiosonde density measurement. Using 4 $RadErr^2$ assumes that the errors due to the radiosonde density measurement are not correlated and this is not the case. The $RadErr$ term includes both random and systematic errors. Systematic radiosonde errors are likely to be correlated between the bottom, r_1, and top, r_2, of a layer implying that 2 $RadErr^2$ factors are perhaps more appropriate in this equation explaining the use of the $\lesssim$ symbol.

The equations are now developed for the two-way particle optical depth. If one desires to determine the one-way particle optical depth, it is necessary to use equation 19 to handle the wavelength scaling. The appropriate error equation is this case is essentially one-half of equation 31. Now that the calculation of atmospheric transmission and extinction has been described, meteorological quantities may be derived. These are presented in part II [49] of this paper.

5 Summary

As the number of Raman lidar systems in use in the world has been on the increase recently, particularly in Europe, it seemed an appropriate time to undertake an updated evaluation of the traditional Raman lidar water vapor and aerosol measurements including effects such as the temperature dependence of Raman scattering. Toward that end, this paper is part I of a thorough two-part review of the traditional, single-laser-wavelength, Raman lidar technique for measuring atmospheric aerosols and water vapor. The temperature sensitivity of Raman scattering from water vapor was simulated numerically and used to calculate the temperature sensitivity of a water vapor measurement using a narrow-band optical filter. A 7% change in transmitted intensity was found for a 0.3 nm filter between 200 K and 300 K. Because of this general temperature sensitivity of Raman scattering, new forms of the elastic and Raman lidar equations were developed that permit the temperature sensitivity of these equations to be considered as a multiplicative factor times the traditional lidar equations. The calculation of atmospheric transmission was discussed in detail. Significant differences were found in calculations of molecular extinction and Rayleigh backscatter coefficient by including the effects of the dispersion of depolarization. The calculation of the differential transmission factor required to evaluate the Raman lidar equation was also discussed in detail. The influence of the wavelength scaling of aerosols was considered in these calculations. In part II [49], these temperature dependent equations are used to derive new forms of the

equations for aerosol scattering ratio and water vapor mixing ratio. Computer code that performs the water vapor temperature sensitivity calculations shown in this manuscript is available from the author upon request.

6 Acknowledgements

Support for this activity has come from the NASA Dynamics and Remote Sensing and Radiation Sciences programs as well as the Department of Energy's Atmospheric Radiation Measurements program. The author is grateful for the assistance provided by J. M. Fernandez in the modeling of the Raman water vapor spectrum.

1 Appendix: The Influence of Multiple Scattering on Tropospheric Aerosol Extinction Measurements

In considering light scattering by particles of the same dimension or larger than the wavelength of the incoming light, as the particle size increases, forward-scattered light is confined to an increasingly narrow angular cone. This makes it more likely that a photon that is scattered forward in a first scattering event will interact with another particle (the second scattering event) and be backscattered within the field of view of the lidar receiver.

The lidar equations formulated earlier were for single scattering only. Therefore, in the case of scattering involving large particles where multiple scattering is more likely to occur, the use of the single scattering equations can lead to errors in the calculated quantities. Most of the quantities derived from Raman lidar data are based on ratios of lidar signals where the multiple scattering influence tends to cancel in the ratio [50]. Examples of these quantities are the water vapor mixing ratio, liquid water mixing ratio, aerosol scattering ratio and the aerosol backscatter coefficient. However, aerosol extinction and optical depth are calculated using only a single lidar signal (e.g. Raman nitrogen) and, in the case of large particles, can be significantly influenced by multiple scattering.

The influence of multiple scattering on lidar signals is related to the optical depth of the scattering medium, the size of particles that are doing the scattering and the range to the scattering volume. The formulation developed by Eloranta [51] will be used here to study this influence. A description of the equations used here has been published recently for the case of Raman lidar measurements of cirrus cloud multiple scattering [7].

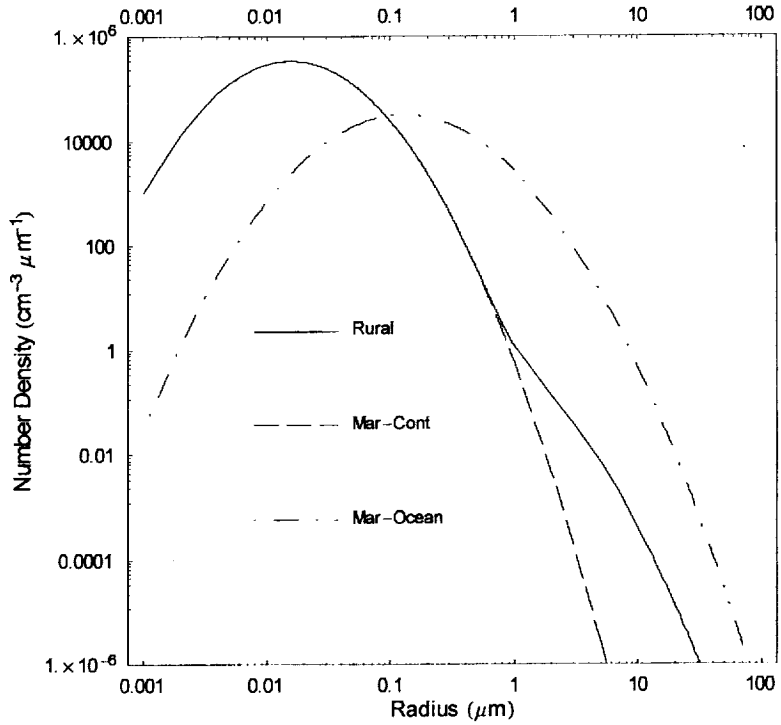

Figure 7: Three AFGL aerosol size distribution models are represented: rural, maritime with aerosols primarily of rural origin, and maritime with aerosols primarily due to sea salt spray. These distributions are appropriate for 70–80% relative humidity.

1.1 Aerosol size distributions

The Air Force Geophysics Laboratory (AFGL) size distribution models for rural and maritime aerosols [52] are presented here. The distributions are represented by one or a sum of two log normal distributions [52]. The results are plotted in figure 7 for rural, maritime with aerosols of primarily rural origin, and maritime with aerosol primarily due to sea salt spray.

Maritime aerosols which originate from sea salt spray are considerably larger on average than either the rural or the maritime continental aerosols. The maritime continental model is identical to the rural model except in the large particle portion of the distribution where the influence of the larger marine aerosols can be seen. These aerosol models are considered representative of the types of aerosols that were likely present at Andros Island, Bahamas during the CAMEX-3 campaign.

1.2 Multiple scattering by atmospheric aerosols

Three synthetic profiles of aerosol extinction were created to study the influence of multiple scattering on the measurement of

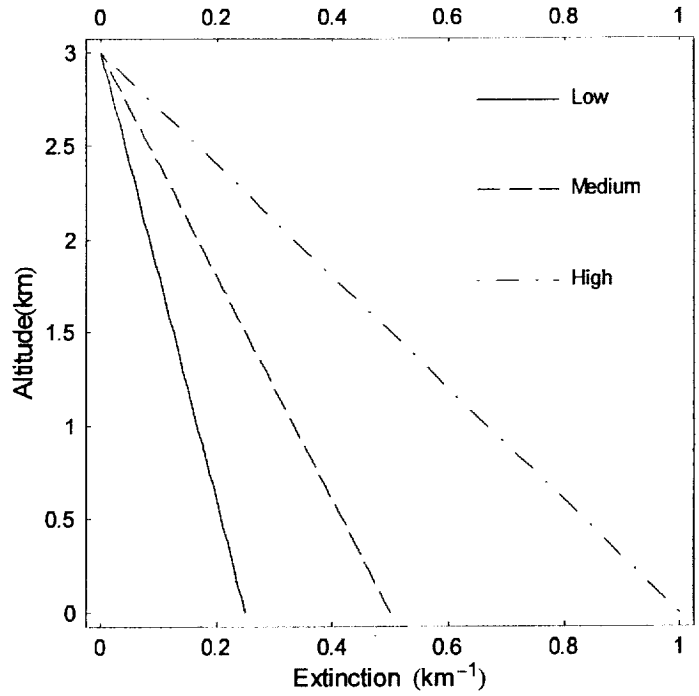

Figure 8: Three synthetic aerosol extinction profiles created to test multiple scattering influence on measurements of aerosol extinction.

extinction using Raman lidar and are shown in figure 8. They have aerosol optical depths of 0.375, 0.75 and 1.5, respectively, to simulate low, medium and high aerosol loading.

Second order multiple scattering was calculated for the three extinction profiles shown in figure 8 assuming that the aerosol particles were of constant radius throughout the profile. To study the possible influence of multiple scattering on the extinction measurements at Andros Island, aerosols of two radii were studied: 0.5 microns and 2.0 microns. The results are shown in figure 9 with the 0.5 micron calculations on the left and the 2.0 micron calculations on the right.

The multiple scattering due to the 0.5 micron aerosol is considerably smaller than that for the 2 micron aerosol. Considering the 2 micron results shown on the right, it can be seen that at the peak of the high aerosol optical thickness case, the ratio of second order scattering to single scattering is less than 3%. At most ranges and for most aerosol conditions, the ratio is considerably less than this. The error in extinction and optical depth due to second order multiple scattering is quantified simply as $\ln\left[P_2/P_1\right]/2$ assuming a wavelength scaling parameter of $k = 1$ where P_2 and P_1 are the probabilities of second and first order scattering, respectively. This implies that the error in the calculation of extinction (see section 4.2) due to second order multiple scattering

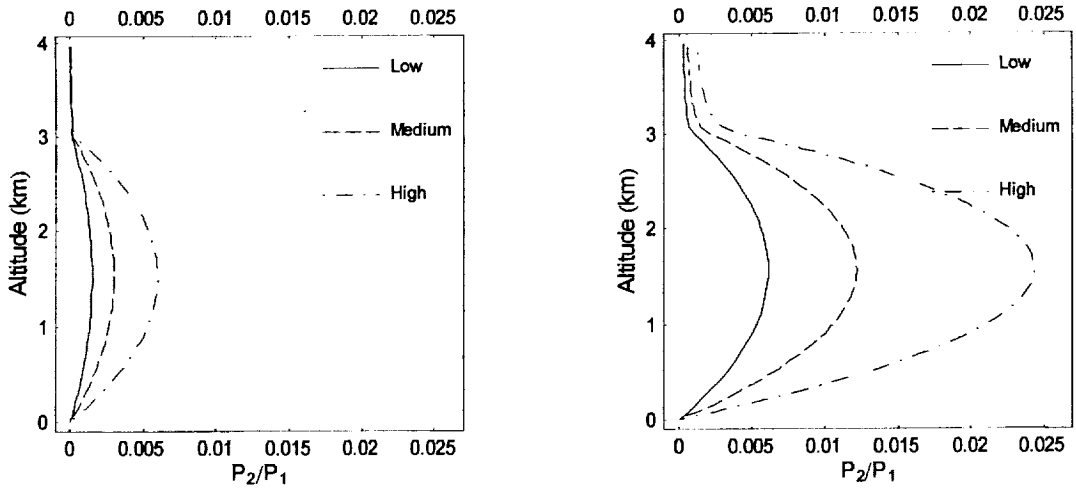

Figure 9: Multiple scattering influence on measurements of extinction due to tropospheric aerosols. Calculations assuming constant size aerosols of 0.5 micron radius are shown on the left and 2.0 microns on the right.

from 2 micron size aerosols will be at most 1.5% and usually much less than this for the cases studied here. Third order scattering will be completely insignificant due to its much lower probability than second order scattering.

The marine oceanic model peaks at 0.3 microns and predicts that there are only 51% and 1.8% as many particles of radii 0.5 and 2 microns, respectively as at the peak. For larger particles than 2 microns, the abundance drops exponentially. Therefore, due to the relative lack of large particles that these model calculations predict for tropospheric aerosols and the generally small effect that multiple scattering has on the calculation of aerosol extinction, multiple scattering has been ignored in the aerosol extinction calculations presented in this paper. However, for the case of denser media such as clouds [50] [5] [7] multiple scattering is an effect that must be considered for a proper evaluation of extinction and optical depth.

2 Appendix: Photon pileup correction

Raman lidar systems frequently make use of photon counting data acquisition systems due to the weak nature of Raman scattering. For example, all of the data acquired by the SRL during CAMEX-3 used photon counting electronics. Photon counting electronics have a certain minimum pulse pair resolution time which, in the case of the 100 Mhz DSP Technology units used in the SRL during the CAMEX-3 campaign, was approximately 10 ns. The maximum measurable count rate corresponding to this is 100 MHz. However, this maximum count rate will be obtained only for a perfectly periodic input pulse train. The Raman lidar

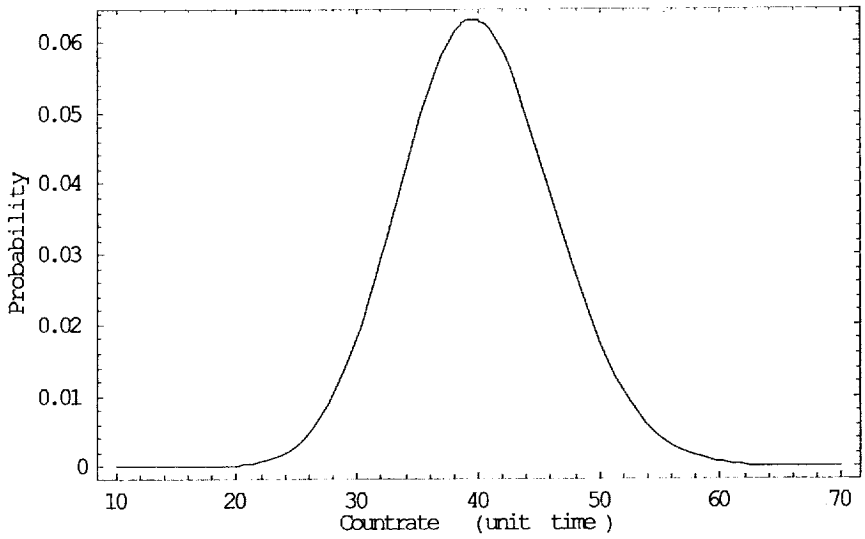

Figure 10: Probability of measuring n counts for a Poisson process characterized by a mean countrate of 40 counts per unit time.

photon counting signals obey Poisson statistics and thus, for a certain mean count rate over a one-minute data acquisition time, the effective countrate for each laser pulse can vary significantly. For example, using a 1 μsec binwidth in the photon counters, a 40 MHz signal would correspond to 40 counts in a bin. The Poisson probability distribution for n counts with μ mean is given by

$$P(n,\mu) = \frac{e^{-\mu}\mu^n}{n!} \tag{B.1}$$

where $P(n,\mu)$ is the probability of measuring n counts in a time interval where the mean number of counts per time interval is μ. Figure 10 shows this distribution with mean of 40. From this figure, it is clear that the effective count rate of the signal from each laser pulse can deviate significantly from the 40 MHz average. Thus, from pulse to pulse, there is a varying probability that two pulses may arrive sufficiently closely spaced in time to be seen as a single event by the electronics.

Traditionally, there are two extremes of behavior that counting systems can exhibit. They are referred to as "paralyzable" and "non-paralyzable" [53]. A paralyzable counting system is one which is unable to provide a second output pulse unless there is a time interval of at least τ between two successive input pulses. If an additional pulse arrives during the response time τ, known as the deadtime, the deadtime of the apparatus is further extended by τ. In this way, at high count rates, the unit will be unable to respond and will be "paralyzed". Since the fraction of intervals that are longer than τ is given by $e^{-\tau N_{real}}$, the equation which relates the measured and true counting rates for a paralyzable counter is [53]

$$N_{measured} = N_{real} e^{-\tau N_{real}} \tag{B.2}$$

where $N_{measured}$ is the observed countrate and N_{real} is the actual countrate.

A non-paralyzable counter is one in which the response time τ is independent of the arrival of additional counts. In other words, a non-paralyzable counting system will asymptotically approach a maximum counting rate as the actual countrate increases. The equation describing the relationship of the measured countrate and the true countrate can be derived as follows. For an observed countrate of $N_{measured}$, the fraction of time that the counting unit is unable to respond to counts is $\tau N_{measured}$, since each observed count will produce a single deadtime period. Thus the fraction of time that the unit is sensitive to counts is $1 - \tau N_{measured}$. The measured countrate may then be expressed as [53]

$$N_{measured} = (1 - \tau N_{measured})\, N_{real} \tag{B.3}$$

or

$$N_{real} = \frac{N_{measured}}{(1 - \tau N_{measured})} \tag{B.4}$$

These two types of counting systems have traditionally been considered extremes of behavior such that the response of a real system would lie somewhere in between. The two curves representing the paralyzable and non-paralyzable corrections are plotted in figure 11 using $\tau = 10\ ns$. For reference, a purely linear response is also shown.

If the countrates are kept low (less than approximately 10-20 MHz in this example), the two equations give similar results. The following example illustrates the use of the non-paralyzable equation. In order to implement any count saturation correction scheme, one must determine the resolving time of the electronics. In a 100 MHz photon counting system, one would expect that the resolving time parameter would be approximately 10 ns. The resolving time value can be determined empirically from two sets of atmospheric profiles: 1) full strength profiles 2) profiles acquired with a 10% neutral density filter in front of all PMTs. The non-paralyzable pulse pileup correction is first applied to both the full and reduced-strength signals which then allows the resolving time value to be determined for each PMT. Figure 12 shows the ratio of the count-corrected, reduced intensity profiles to the count-corrected, full-strength profiles in the high nitrogen channel for resolving times of 8, 10, 12, and 14 ns. To produce the ratios shown in the figure, the background must be subtracted from each signal. In addition, the reduced intensity and full

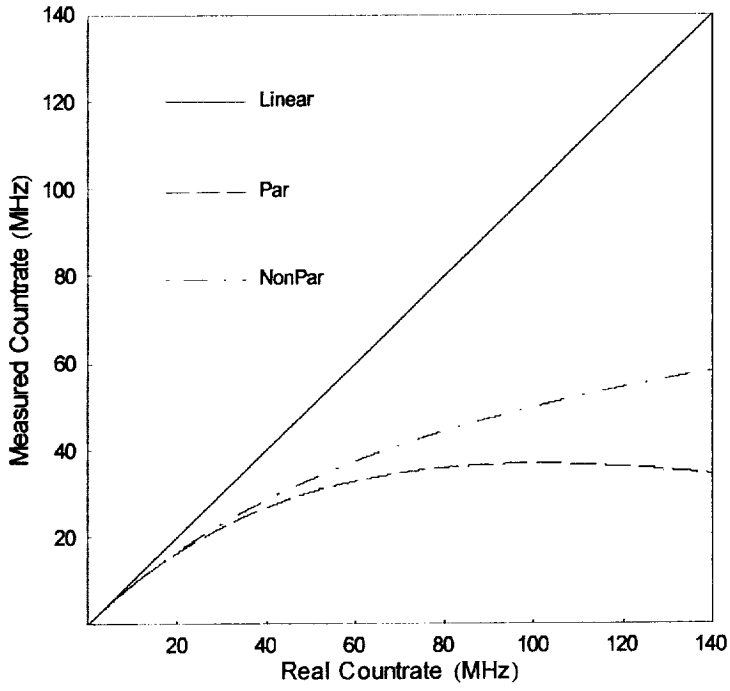

Figure 11: Comparison of paralyzable and non-paralyzable count corrections. The observed count rate of a paralyzable system tends toward zero with increasing true count rate. The observed count rate of a non-paralyzable system tends toward the maximum countrate as the real count rate increases. A perfect linear system is also represented.